# Self-Attention based Cloud Top Height Retrieval for Intelligent Meteorological Service Recommendation

Xuhao Shi[a], Jie Zhang[b,*], Guoqiang Liu[a], Kun Yi[c,d], Muhammad Bilal[e]

[a]*School of Software, Nanjing University of Information Science & Technology, China*
[b]*Shanghai Meteorological Information and Technology Support Center, Shanghai, China*
[c]*North China Institute of Computing Technology, China*
[d]*State Information Center of China, China*
[e]*School of Computing and Communications, Lancaster University, UK*

**Abstract**

Recommendation systems are widely applied across various domains, particularly in providing users with personalized content and service recommendations. However, traditional recommendation systems face challenges in meteorological services when handling complex atmospheric data and real-time dynamic user needs. Accurate cloud top height (CTH) retrieval is crucial for enhancing meteorological services, especially in delivering precise weather forecasts and warnings. This paper proposes a self-attention-based CTH retrieval model integrated into an intelligent meteorological service recommendation (IMSR) system. Leveraging self-attention mechanisms, the model captures long-range dependencies and extracts key global features from satellite-based meteorological data, improving the accuracy of CTH retrieval even in data-sparse environments. Additionally, the system utilizes real-time CTH data to provide personalized weather recommendations for agriculture, transportation, and tourism users. Experimental results demonstrate that the proposed model outperforms existing methods in both CTH retrieval accuracy and recommendation effectiveness, significantly enhancing the timeliness and relevance of meteorological services. This approach integrates advanced deep learning techniques with practical applications in weather services, offering potential for cross-domain applications.

*Keywords:* Intelligent Meteorological Service Recommendation, Cloud top height retrieval, CRU-RecNet, Self-attention mechanism

## 1. Introduction

Recommendation systems are widely applied in various industries, offering personalized content and services based on user preferences and behaviors [1]. In meteorological services, the demand for customized weather forecasting has increased significantly, as industries such as agriculture, transportation, and tourism rely heavily on accurate and timely weather information to optimize operations and ensure safety [2]. Unlike traditional forecasting systems, recommendation systems analyze user-specific data, such as location and activity preferences, to deliver tailored weather suggestions [3]. For instance, a farmer can receive guidance on the best irrigation times based on localized weather data. At the same time, a traveler might be warned of potential delays caused by adverse weather conditions [4]. In transportation, precise weather information is crucial to managing traffic flows, reducing delays, and ensuring

Email addresses: s837731501@gmail.com, jzhangchina@126.com, bwq0709@gmail.com, kunyi.cn@gmail.com, m.bilal@ieee.org
*Corresponding author

passenger safety. However, the dynamic nature of meteorological data introduces unique challenges for recommendation systems, requiring them to adapt quickly to changing conditions [5].

Cloud top height (CTH) refers to the vertical distance between the top of a cloud and the Earth's surface [6], providing critical insights into cloud structure and atmospheric stability. CTH plays a key role in identifying areas of atmospheric instability, which are often precursors to extreme weather events like thunderstorms, hurricanes, and hail [7]. For instance, high CTH values usually indicate strong convective activity, signaling the potential for hazardous conditions. This parameter is not only fundamental in meteorology but also impacts industries such as agriculture, aviation, and disaster management. In aviation, for example, CTH data helps pilots avoid dangerous weather zones, ensuring flight safety, while in agriculture, it assists farmers in assessing precipitation risks and optimizing irrigation schedules [8].

However, obtaining accurate CTH data under complex atmospheric conditions remains challenging. Traditional CTH retrieval methods include radiometric techniques and satellite imaging [9]. Active remote sensing techniques, such as lidar, directly measure the physical properties of the cloud with high accuracy. However, their low spatiotemporal resolution and limited coverage hinder large-scale real-time monitoring [10]. Passive remote sensing, on the other hand, uses different wavelengths of natural radiation to infer CTH, providing continuous observations and broad coverage. However, the CTH retrieval models based on passive remote sensing data involve Radiative Transfer Models (RTMs), and the effectiveness of RTMs is compromised when solar radiation is lacking as a source of reflected light [11]. Moreover, RTMs face numerous challenges when dealing with optically thin clouds, cirrus clouds, or broken clouds. The radiation signals from these cloud types are relatively weak, and their scattering and absorption effects on light are difficult to accurately simulate. Capturing and analyzing them precisely is particularly challenging, making it extremely difficult to obtain accurate and usable CTH data [5][12].

In addition, traditional recommendation systems face challenges in processing complex, dynamic meteorological data in real-time [13][14]. The multidimensional and real-time nature of meteorological data requires recommendation systems to quickly adapt to changing weather conditions to provide accurate personalized services. Traditional systems, however, often fall short of meeting this need, which limits the applicability of intelligent meteorological services in agriculture, transportation, and tourism [15].

To address these challenges, this study proposes a novel CTH retrieval model based on multi-scale attention and self-attention mechanisms[16], which is integrated with an intelligent meteorological service recommendation (IMSR) system, simultaneously solving the problems of low model availability under complex weather conditions and nighttime scenarios. We replaced the traditional single-scale convolution with a multi-scale attention module (MAM) and a convolutional block attention module (CBAM) to overcome the limitation of the model's ability to handle complex cloud layer structures. The MAM employs dilated convolutions with different sampling rates to capture cloud layer features at different scales, while CBAM adaptively suppresses interfering features. These designs enable the model to effectively extract features even under challenging conditions, such as optically thin layers, without requiring additional observation channels. To address the limited receptive field of traditional convolutional networks, we utilize a three-layer parallel self-attention structure to establish global associations between pixels and capture long-range dependencies between infrared channels. Specifically, we use dynamic attention weight adjustments to enhance the model's global feature perception capability and adopt a novel dual-decoder architecture to balance global semantic information and local detail preservation. The CTH data obtained will ultimately serve as a critical input for the recommendation system, allowing the provision of customized and real-time meteorological services for industries such as agriculture, transportation, and tourism [17].

The contributions of this paper are as follows:

- Development of a self-attention-based CTH retrieval model that significantly improves prediction accuracy and robustness through a novel architecture combining multi-scale attention and self-attention mechanisms. Unlike traditional convolutional networks, our model effectively captures long-range dependencies between infrared channels and adaptively focuses on key atmospheric features.

- Introduction of a unique dual-decoder architecture that balances global semantic information and local detail preservation, enabling more accurate detection of complex cloud structures even in optically thin cloud layers and cirrus clouds where traditional radiative transfer models struggle. This innovative approach addresses the limitations of fixed receptive fields in conventional CNNs without significantly increasing computational complexity.

- Implementation of a highly effective CTH retrieval system for low-light and nighttime scenarios, where our model maintains superior performance (as validated with CALIPSO nighttime data) through dynamic attention weight adjustments that enhance the model's global feature perception capability even when solar radiation is lacking—a significant advantage over traditional passive remote sensing methods.
- Integration of the high-precision CTH retrieval with an intelligent meteorological recommendation system using collaborative filtering, establishing a novel pipeline for delivering personalized, real-time weather forecasting services that adapt to dynamic user needs across agriculture, transportation, and tourism sectors.

The structure of this paper is as follows: Section 2 reviews related literature, focusing on the limitations of traditional CTH retrieval techniques and the use of self-attention mechanisms in meteorological applications. Section 3 details the design of the CRU-RecNet model and discusses the limitations of current methods. Section 4 describes the experimental setup, evaluation metrics, and results. Finally, Section 5 summarises key findings and concludes the study.

## 2. Related Work

In recent years, with the development of machine learning, particularly deep learning techniques, significant progress has been made in CTH retrieval and IMSR. Many studies have focused on improving retrieval accuracy through innovative model architectures and feature extraction methods. Meanwhile, the application of recommendation systems in meteorological services has become increasingly sophisticated, incorporating more advanced algorithms to provide personalized and accurate weather services. In this section, we review the key research works on CTH retrieval models and recommendation system technologies, highlighting the progress made and the challenges encountered in real-world applications.

### *2.1. U-Net*

U-Net is a deep learning network specifically designed for image segmentation [18]. Since its introduction in 2015, it has gained widespread popularity due to its exceptional performance. Its unique feature is the symmetric U-shaped architecture, where deep features from the encoder are directly transferred to the decoder through skip connections, effectively restoring image details and enabling precise pixel-level predictions. This design allows U-Net to excel in scenarios with limited annotated data, such as medical image segmentation. It has also been widely applied in satellite image processing and industrial image analysis. By integrating multi-scale features, U-Net optimizes segmentation quality, demonstrating strong capability and flexibility in handling complex image tasks.

### *2.2. Deep Learning models for CTH retrieval*

In recent years, in addition to U-Net applications in CTH data retrieval, other deep learning models such as Convolutional Neural Networks (CNNs), Generative Adversarial Networks (GANs), and Residual Neural Networks (ResNet) have shown significant potential in this field. Convolutional Neural Networks (CNNs) have been widely applied in extracting multi-scale features from CTH data, demonstrating excellent performance in identifying complex cloud structures [19]. Through hierarchical convolution operations, CNNs can capture spatial structures and scale variations within multi-channel satellite data, thereby improving the accuracy of CTH predictions, particularly under extreme weather conditions [20]. Generative Adversarial Networks (GANs) have also garnered attention in CTH retrieval due to their powerful data generation capabilities. GANs can generate realistic synthetic images to compensate for observation gaps under low-light or night conditions, enabling high accuracy in CTH retrieval even in data-sparse scenarios. Recent studies indicate that GAN-generated data significantly enhance cloud detection accuracy in complex atmospheric conditions [21]. Residual Neural Networks (ResNet), by introducing residual connections, effectively address the gradient vanishing problem in deep networks, making them highly efficient and stable for deep feature extraction. In CTH retrieval, ResNet efficiently learns multi-level cloud features, improving the precision of cloud-top height predictions [22]. Additionally, ResNet has shown superior performance in handling complex cloud structures and stratified atmospheric features, helping accurately capture essential meteorological data characteristics. The incorporation of these deep learning models not only expands the technical approaches to CTH data analysis but also significantly enhances model accuracy and robustness under complex weather conditions, providing stronger theoretical and technical support for CTH retrieval.

### 2.3. Attention Mechanisms in Recommendation Systems

In recent years, attention mechanisms have become a pivotal element in recommendation systems, especially for capturing user behavior patterns and enhancing personalized recommendations. Self-attention models are widely used due to their ability to identify long-range dependencies and contextual information, which are crucial for accurately predicting user preferences. For instance, Qi et al. (2019) introduced a time-aware distributed service recommendation approach that integrates privacy preservation, providing a robust framework for sensitive user data in recommendation systems [23][24]. In a more recent study, Liu et al. (2024) proposed a dynamic embedding transportation model, enhancing cross-domain recommendation accuracy through adaptive feature alignment [1]. Attention-based architectures have continued to evolve. For example, Sun et al. developed BERT4Rec, a bidirectional self-attention model that can capture both past and future contexts in user sequences, achieving superior performance for next-item prediction [25]. Similarly, Chen et al. (2024) designed a transformer-based recommendation system specifically for e-commerce, where user interest often fluctuates rapidly. Their work underscores the ability of self-attention mechanisms to capture short-term user preferences for real-time personalized recommendations dynamically [26]. Additionally, Zhou et al. (2018) introduced the Deep Interest Network (DIN), which utilizes attention mechanisms to model shifts in user interests, further refining recommendation accuracy [27]. To expand on this, Xu et al. (2024) proposed a cross-attention mechanism that jointly analyses user and item features in collaborative filtering, significantly improving the contextual relevance of recommendations by capturing intricate user-item relationships [28][29]. These recent advancements illustrate how self-attention and attention-based mechanisms have continued to drive innovation in recommendation systems. By integrating adaptive models capable of handling complex and dynamic user behavior patterns, these methods have demonstrated substantial improvements in recommendation accuracy and responsiveness, keeping the field in line with the latest technological advancements.

### 2.4. Reinforcement Learning in Intelligent Services

Reinforcement Learning (RL) has been widely adopted in intelligent services, particularly for resource allocation and dynamic decision-making tasks. Xu et al. proposed XRL-SHAP-Cache, a model that combines explainable AI with reinforcement learning to optimize edge caching in content delivery networks (CDNs) [30][31]. The use of SHAP (Shapley Additive Explanations) in this model improves system transparency and user trust by explaining the model's decision-making process. In the realm of autonomous driving and intelligent transportation, RL is increasingly applied to optimize resource allocation for connected and automated vehicles. Xu et al. introduced a multi-agent reinforcement learning-based distributed edge caching method designed for zero-trust environments in connected vehicles [32]. This method leverages cooperation among RL agents to optimize resource scheduling and caching strategies. RL has also been applied in content recommendation systems. Zhao et al. developed a Page-Level Recommendation system based on deep reinforcement learning, which dynamically adjusts recommendation strategies to improve long-term user satisfaction [33]. Similarly, Ali et al. introduced RLRec, a deep RL-based recommendation system that optimizes long-term rewards to improve recommendation performance [34]. Liu et al. proposed DRN (Dynamic Recommendation Network), which adapts recommendation strategies in real-time based on user feedback using RL techniques [35]. In the smart home context, RL has been applied to provide personalized service recommendations. Mohammadi et al. demonstrated that RL could be used to optimize smart home device control, improving user comfort and quality of life [36]. These studies demonstrate the potential of RL in optimizing resource allocation, improving recommendation accuracy, and dynamically adjusting recommendation strategies in intelligent services.

In summary, recent years have seen significant progress in the fields of CTH retrieval and IMSR. Deep learning techniques, especially convolutional neural networks like U-Net and self-attention mechanisms, have proven effective in atmospheric data processing and recommendation systems. These methods have shown great potential in improving the accuracy of CTH retrieval and the effectiveness of personalized recommendation services. However, despite these advancements, existing models still face challenges in addressing global dependencies across multi-source data, data sparsity, and the dynamic nature of user preferences. Therefore, effectively integrating CTH retrieval with intelligent recommendation services to further enhance recommendation precision and user experience remains a key direction for future research.

## 3. CRU-RecNet model for IMSR

This section introduces the CRU-RecNet model, which leverages multi-scale attention and self-attention mechanisms to predict CTH and provide IMSR accurately. As shown in Figure 1, the CRU-RecNet architecture is based on the U-Net framework. It consists of five key components: the encoding module, the small decoder module, the large decoder module, the connection module, and the recommendation module. The encoding module is responsible for extracting deep semantic information from satellite data, capturing essential atmospheric features and cloud structures, which are crucial for CTH prediction. The self-attention module (SAM) and MAM are embedded within the Bridge, enhancing CRU-RecNet's ability to capture multi-level atmospheric patterns and complex cloud structures. These attention mechanisms enable the model to perform a more detailed and precise analysis of cloud structures, improving the accuracy of CTH retrieval, which is essential for accurate weather forecasting. The decoding process progressively reconstructs CTH predictions through cross-layer connections, similar to how meteorological systems integrate data at various stages to improve forecast accuracy. By leveraging multi-level integration, the final CTH predictions become more accurate and refined. The Recommendation utilizes these high-precision CTH data to generate personalized weather forecasts and actionable recommendations for users across industries such as agriculture, transportation, and tourism.

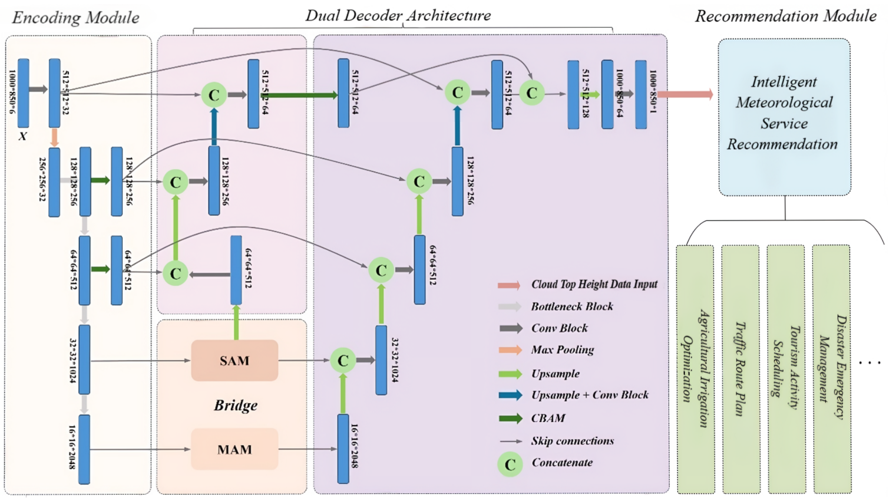


Figure 1: CRU-RecNet model framework diagram

Once the CTH data is accurately reconstructed, it serves as input for IMSR systems. These high-precision CTH predictions enable the generation of personalized weather forecasts and recommendations, supporting more informed decision-making across various industries. For example, agricultural users can adjust irrigation schedules based on CTH data. At the same time, transportation services can optimize routes by incorporating cloud height information, thus enhancing both the practicality and personalization of meteorological services.

### 3.1. Encoding Module

The encoding module adopts the ResNet-50 setup [37], uses five rounds of downsampling to reduce the resolution, and gradually extracts the deep semantics. The first round of downsampling contains a convolutional layer with the size of $7 \times 7$ and a maximum pooling layer. The computational formulas are shown in Equation (1) and Equation (2):

$$Z = BN\left(W_{7\times 7} * X\right), \tag{1}$$

$$T = \mathrm{MaxPool}(\mathrm{ReLu}(Z)), \tag{2}$$

where $BN$ denotes the batch normalization layer, which serves to maintain the consistency of the distribution of the data in each layer to avoid the problem of disappearing or exploding gradients during the training process. $X$

denotes satellite multichannel data, $W_{7\times7}$ denotes the convolution of size $7 \times 7$, T denotes the output of this round of downsampling, and *MaxPool* and *ReLu* denote the maximum pooling layer and the *ReLu* activation function, respectively.

The second through fifth rounds of downsampling used the Bottleneck Block as the basic unit, with the second round of downsampling containing three bottleneck blocks. The third round of downsampling used four bottleneck blocks. The fourth round of downsampling used six bottleneck blocks. The fifth bottleneck layer uses three bottleneck layers. The formulas for the bottleneck layers are shown in Equation (3), Equation (4), and Equation (5):

$$T_1 = ReLu(BN(W_{1\times1} * T)), \tag{3}$$

$$T_2 = ReLu(BN(W_{3\times3} * T_1)), \tag{4}$$

$$S = ReLu(BN(W_{1\times1} * T)) + ReLu(BN(W_{1\times1} * T_2)), \tag{5}$$

where $W_{1\times1}$ denotes the convolution of size $1 \times 1$ to adjust the channel data of the feature map.$W_{3\times3}$ denotes the convolution of size $3 \times 3$. S denotes the output of the bottleneck layer. Residual concatenation by convolution of size $1 \times 1$ can effectively reduce the number of parameters and computational complexity while maintaining the network performance.

### *3.2. Dual Decode Architecture*

To address the challenges of capturing both large-scale atmospheric patterns and fine-grained cloud structure details, a dual-decoder structure is proposed. High-level features extracted through multi-layer down-sampling possess a broad receptive field and are adept at representing large-scale atmospheric patterns. However, they lack the resolution necessary to capture detailed cloud formations. Conversely, low-level features offer higher resolution and are better suited for capturing localized cloud behavior but are limited in their ability to represent broader atmospheric patterns. The dual-decoder structure leverages the strengths of both feature types, ensuring the preservation of global atmospheric context while enhancing the model's ability to recover fine-grained details. This design improves CTH retrieval accuracy and provides precise input for personalized meteorological service recommendations.

The large decoder employs a total of five rounds of up-sampling to recover the information of the feature maps gradually. The formula for each round of up-sampling is shown in Equation (6):

$$O = W_{3\times3} * Concat(DConv(\mathrm{t}), X_{pre}), \tag{6}$$

where $W_{3\times3}$ denotes the convolution of dimension $3 \times 3$, *DConv* denotes the transposed convolution, $X_{pre}$ denotes the spanning connection from the previous layer, $O$ denotes the output of the current round of down-sampling, and $t$ denotes the output features from the Bridge or the last round of down-sampling. *Concat* then denotes splicing along the channel dimension.

By integrating outputs from the first four levels of feature maps, as well as the SAM and MAM, the large decoder effectively extracts multi-scale contextual information. This information is then progressively restored to the original resolution through up-sampling, preserving global semantic information.

The small decoder focuses on recovering fine edge details from low-level feature maps and refining the output of the large decoder. It conducts a three-stage up-sampling operation, beginning with up-sampling features refined by SAM. These are then merged with the feature maps optimized by CBAM along the channel dimension. Finally, a convolutional layer adjusts the number of channels in the merged feature maps to align with subsequent processing requirements. Each up-sampling step is represented by Equation (7):

$$O = W_{3\times3} * Concat(CBAM(X_{pre}), DConv(t)), \tag{7}$$

where $X_{pre}$ denotes the skip connection from the previous layer, $O$ denotes the output of the current downsampling round, and $t$ is the output features from the connection module or the previous downsampling round.

The dual-decoder structure combines the strengths of high-level and low-level features: the large decoder captures global atmospheric patterns, while the small decoder ensures the accurate recovery of fine-grained edge details. This synergy enhances the accuracy of CTH retrieval and provides robust, detailed inputs for intelligent meteorological recommendations.

### 3.3. Multi-scale Attention Module

CTH data exhibits significant multi-scale characteristics, making it crucial to accurately extract atmospheric features at different scales to improve the performance of CTH retrieval models. Additionally, the complexity of atmospheric data often includes a large amount of noise, and retrieval models need to focus on key atmospheric patterns and cloud structure formations. To enhance the model's ability to extract multi-scale features and to focus on critical patterns in cloud data, this chapter introduces a MAM. The primary objective of this module is to enable the model to more precisely identify and capture cloud features of various sizes and formations while effectively reducing the impact of noisy data on retrieval results. This module enhances the overall model performance without significantly increasing computational costs. The detailed structure of the MAM is shown in Figure 2.

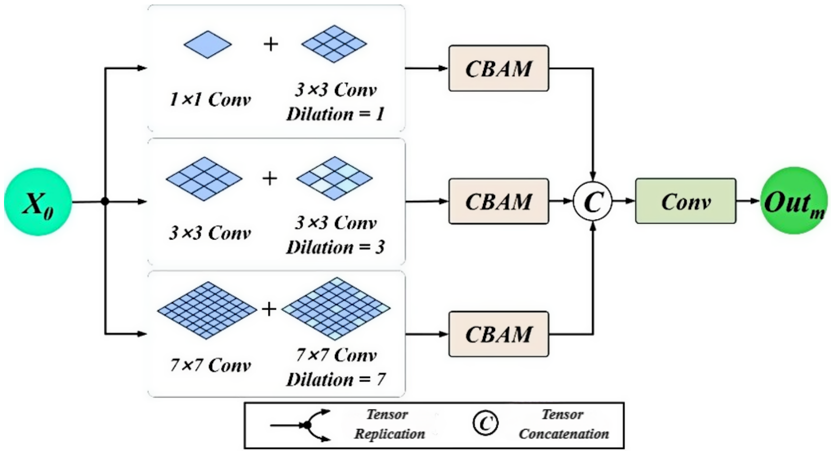


Figure 2: Structure of the MAM

The module first simulates the relationship between the size of the sensory field and the eccentricity using different combinations of convolutions and null convolutions to enhance the distinguishability and robustness of the features. The formulas for this process are shown in Equation (8), Equation (9), and Equation (10):

$$X_1 = W_{1\times1} * X + W_{3\times3D1} * X_0, \tag{8}$$

$$X_2 = W_{3\times3} * X + W_{3\times3D3} * X_0, \tag{9}$$

$$X_3 = W_{7\times7} * X + W_{7\times7D7} * X, \tag{10}$$

where $X_0$ is the output of the encoding module, $W_{n\times n}$ denotes the convolution of size, and $W_{n\times nDK}$ denotes the hollow convolution of size $n \times n$ with dilation $k$.

Subsequently, the key CTH features are augmented with different scale features from both spatial and channel dimensions through the CBAM to filter the interfering features. Finally, after stitching the enhanced features along the channel dimension, the final feature dimensions are adjusted by a convolution of size $3 \times 3$ to get the final module output. This process is represented as Equation (11):

$$Out_m = W_{3\times3} * [CBAM(X_1), CBAM(X_2), CBAM(X_3)]. \tag{11}$$

### 3.4. Self-attention Module

Traditional convolutional networks face limitations in extracting global atmospheric features due to the fixed size of convolutional kernels. Larger kernels extend the receptive field but significantly increase complexity and hinder the ability to capture fine-grained cloud structures. To overcome these challenges, this study introduces a SAM, as illustrated in Figure 3. This module enables the model to capture global dependencies in CTH data without relying on convolutional kernel size, thereby enhancing global feature extraction and improving CTH retrieval accuracy.

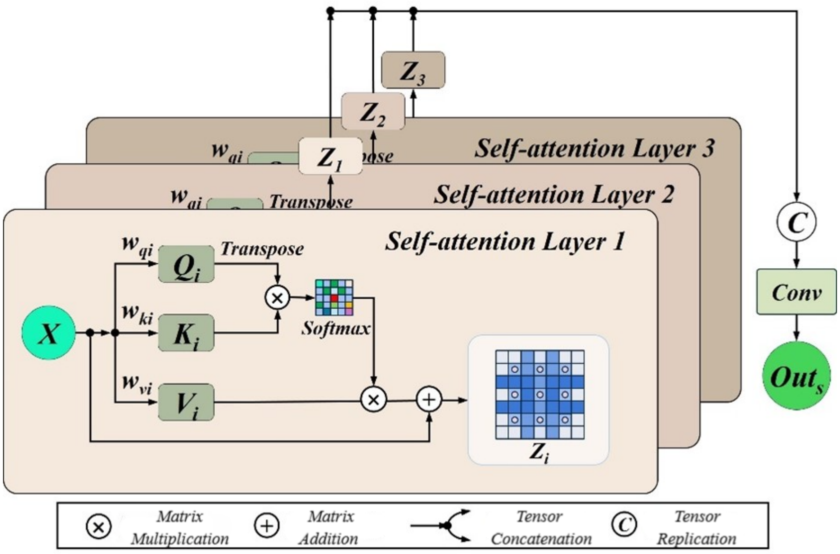


Figure 3: SAM Architecture Diagram

The self-attention mechanism dynamically assigns weights to elements within the feature map, focusing on critical regions and enhancing the model's ability to capture long-range dependencies. This mechanism improves CTH retrieval accuracy by capturing cloud structure relationships, multi-layer features, and temporal dynamics. The attention weights are computed using Equation (12):

$$Attention(Q, K, V) = softmax\left(\frac{QK^T}{\sqrt{d_k}}\right)V, \tag{12}$$

where $Q$, $K$, and $V$ represent query, key, and value matrices derived from input features $X$; the dot product between $Q$ and $K$ is scaled by $\sqrt{d_k}$ to stabilize gradients and normalized with a softmax function to compute the attention weights.

The SAM comprises three layers of self-attention, enabling parallel extraction of multi-scale features from CTH data. Each layer focuses on different levels of information, ranging from local cloud formations to global atmospheric patterns. This design effectively integrates diverse contextual information, enhancing CTH retrieval accuracy.

Each self-attention layer first processes input features using $1 \times 1$ convolutions to generate $Q_i$, $K_i$, and $V_i$. These matrices are used in the self-attention computation shown in Equation (13) to refine global feature information:

$$Z_i = softmax\left(\frac{Q_i K_i^T}{\sqrt{d_{ki}}}\right)V_i. \tag{13}$$

The outputs from all layers are concatenated along the channel dimension and processed by a $3 \times 3$ convolutional layer to fuse multi-layer features. This final step produces the SAM's output, as shown in Equation (14):

$$Out_s = W_{3\times3} * [Z_1, Z_2, Z_3]. \tag{14}$$

The self-attention mechanism significantly enhances the model's capacity to capture long-range dependencies, integrate multi-scale features, and dynamically focus on key regions within the cloud data. By leveraging these improvements, the SAM refines CTH predictions under complex atmospheric conditions, providing more precise inputs for meteorological service recommendations.

### 3.5. Recommendation Module

In the CRU-RecNet model, the recommendation module utilizes collaborative filtering to provide personalized meteorological service recommendations using the retrieved CTH data as input. The core of collaborative filtering lies in analyzing similarities between users or between users and meteorological services to generate the most relevant recommendations for each user. First, the recommendation module obtains high-precision CTH data from the retrieval process, which reflects cloud height variations across different times and regions, providing accurate meteorological insights. The system then combines these CTH data with users' historical behavior data, such as previously queried weather services or behavioral patterns under specific weather conditions, to construct a user-item interaction matrix [38]. In user-based collaborative filtering, the system calculates the similarity between the current user and other users (typically using cosine similarity or Pearson correlation), identifying user groups with similar meteorological needs. Based on these similar users' historical behaviors, the system generates personalized weather service recommendations for the current user. Through this approach, the recommendation system effectively leverages both CTH data and user preferences to offer accurate, real-time meteorological service recommendations for users in fields like agriculture, transportation, and tourism.

## 4. Experimental results and analysis

### 4.1. Experimental environment

This section evaluates CRU-RecNet's performance through comparison and ablation experiments. The environment configurations used in this experiment are detailed in Table 1.

Table 1: Experimental environment configuration

| Matrix | Model (version) |
|---|---|
| Operating system | CentOS7 |
| GPUs | NVIDIA TITAN V |
| CPU | Intel(R) Core(TM) i9-10850k |
| Random access memory (RAM) | 128GB |
| Pytorch | 1.11 |

### 4.2. Experimental datasets

This study focuses on the retrieval of CTH data and its integration with the personalization function of a recommendation system. The goal is to enhance both the accuracy of weather warnings and the overall user experience. To achieve this, the CALIPSO satellite dataset, provided by NASA [39], was selected as the primary data source. This dataset includes detailed observations of cloud layer heights and atmospheric aerosols, leveraging lidar technology to achieve high spatiotemporal resolution. The CALIPSO dataset is particularly well-suited for CTH retrieval under complex atmospheric conditions, such as during thunderstorms and heavy rain, offering precise information on cloud structure and height.

The selected CALIPSO dataset corresponds to the CAL-LID-L2-05kmLay-Standard-V4-21 product, which provides cloud layer data at a 5-kilometer resolution. The V4.21 version incorporates several significant technical advancements. These include the introduction of a Cloud-Aerosol Discrimination (CAD) probability distribution function, which significantly enhances the reliability of cloud and aerosol classification. The dataset also demonstrates improved sensitivity to suspended aerosols, achieving a more accurate classification of high-altitude smoke plumes and Asian dust layers. Moreover, the application of a derivative-based peak-finding algorithm for surface detection allows the dataset to perform well in highly turbid atmospheric conditions while maintaining or improving accuracy under clear-sky scenarios. Additional advancements include the refined handling of strongly scattering layers, which are preserved during coarse-resolution averaging, and special processing for specific anomalies to improve classification accuracy further. These improvements collectively enhance the dataset's utility in atmospheric classification, surface detection, and the provision of scientific information.

The dataset underwent preprocessing to ensure compatibility and quality before being used with the CRU-RecNet model. Missing or abnormal values were removed, and key parameters such as CTH and aerosol optical depth were normalized to improve model convergence and stability [40]. The data were then split into training, validation, and testing sets to ensure a balanced representation across various atmospheric conditions, including daytime, nighttime, and extreme weather events.

The CRU-RecNet model employs multi-scale attention and self-attention mechanisms to prioritize different scale features of cloud layers adaptively. In complex atmospheric environments, particularly at night when there is insufficient light, the model is capable of maintaining high-precision retrieval of CTH. Moreover, the integration of the recommendation system data with the model enhances the efficacy of personalized weather recommendations. The evaluation of the retrieval accuracy employed metrics such as mean square error (MSE), mean absolute error (MAE), and root mean square error (RMSE). In contrast, the assessment of the recommendation system performance utilized metrics such as precision@K and recall@K.

### 4.3. Model parameterization

The retrieval model entails numerous hyperparameters throughout the training phase. These include a training batch size of 8, the utilization of the Adam optimizer, a loss function comprising MSE and MAE, an initial learning rate of 0.001, and a maximum of 80,000 iterations.

In addition, in order to adapt to the characteristics of the ReLU activation function and effectively solve the problem of gradient vanishing and explosion that may be encountered during the model training process, this model adopts the He [41] initialization strategy to set the weights. For a given layer, the weight W initialization is randomly drawn from a normal distribution, the interval of which is shown by Equation (15):

$$W \sim \mathrm{N}\left(0, \sqrt{\frac{2}{n_{in}}}\right), \tag{15}$$

where $\mathrm{N}\left(0, \sigma^2\right)$ denotes the normal distribution with a mean of 0 and a variance of $\dot{\sigma}^2$, and $n_{in}$ denotes the number of nodes in the previous layer.

### 4.4. Evaluation indicators

The experiments in this section used the following metrics to assess the retrieval quality of the retrieval model: MAE, mean bias error (MBE), RMSE, and correlation coefficient (R).

MAE measures the average size of the absolute value of the difference between the predicted and actual values. It is a measure of prediction accuracy that gives the average absolute magnitude of the prediction error. The smaller the MAE, the higher the prediction accuracy of the model. The MAE gives the same weight to all error magnitudes and is calculated as shown in Equation (16):

$$\mathrm{MAE} = \frac{1}{n}\sum_{i=1}^{n} |y_i - \hat{y}_i| \,. \tag{16}$$

MBE measures the average degree of deviation of the predicted values from the actual values and reflects the systematic over- or underestimation of the expected values. Positive values indicate that the predicted values tend to systematically overestimate the exact values, while negative values indicate systematic underestimation. MBE can be used to detect the direction of bias in the model's predictions, and the formula is shown in Equation (17):

$$\mathrm{MBE} = \frac{1}{n}\sum_{i=1}^{n} (y_i - \hat{y}_i) \,. \tag{17}$$

RMSE measures the square root of the squared mean of the differences between predicted and actual values. It gives higher weight to larger errors and is, therefore, often used to emphasize the unacceptability of larger deviations. The smaller the RMSE, the higher the predictive accuracy of the model. The formula is shown in Equation (18):

$$\mathrm{RMSE} = \sqrt{\frac{1}{n}\sum_{i=1}^{n} (y_i - \hat{y}_i)^2}. \tag{18}$$

The R measures the degree of linear correlation between predicted and actual values. Its value ranges from -1 to 1, where 1 indicates a perfect positive correlation, 0 means no linear correlation, and -1 indicates a perfect negative correlation. R provides information about the strength and direction of the relationship between the predicted and actual values and is calculated using the formula shown in Equation (19):

$$R = \frac{\sum_{i=1}^{n}(y_i - \overline{y})(\hat{y}_i - \overline{\hat{y}})}{\sqrt{\sum_{i=1}^{n}(y_i - \overline{y})^2 \sum_{i=1}^{n}(\hat{y}_i - \overline{\hat{y}})^2}}. \tag{19}$$

### 4.5. Comparative experimental results and Analysis

In the study by Wang et al. [42], it has been demonstrated that the deep learning-based retrieval model outperforms the physical method-based retrieval model for the same dataset. Therefore, the comparison experiments in this section select representative deep learning models from previous work on CTH retrieval based on geostationary meteorological satellites to compare with the proposed CRU-RecNet model, which mainly includes U-Net [43], RESU-Net [44]U-Net, RESU-Net, and DNN [42]. U-Net is a classical convolutional neural network structure, the overall architecture is divided into two parts, encoder and decoder, and combines low-level and high-level features through jump connections, which has been widely used in image segmentation tasks. RESU-Net, on the other hand, is an improvement of U-Net and employs residual connectivity to improve the training stability and performance of the model. DNN, on the other hand, uses two rounds of up-sampling and two rounds of down-sampling, as well as a fully connected layer structure to invert satellite data.

Table 2: Experimental quantitative evaluation results of different models on the test set

| **Model name** | **MAE** | **MBE** | **RMSE** | **R** |
|---|---|---|---|---|
| U-Net | 0.894 | -0.265 | 1.416 | 0.946 |
| RESU-Net | 0.772 | -0.258 | 1.125 | 0.969 |
| DNN | 0.906 | -0.341 | 1.562 | 0.938 |
| CRU-RecNet | **0.682** | **-0.136** | **0.893** | **0.982** |

Table 2 shows the quantitative evaluation results of CTH retrieval on the test set for all the models in the comparison experiments in this section, where the lower MAE proves that the model performs better on the test set, MBE is greater than 0, the model overestimates the CTH, and the lower than 0, the model underestimates the CTH, and the closer the value is to 0, the better the model performs on the test set. The lower RMSE proves that the model performs better on the test set. The closer the RMSE is to 1, the better the model performs on the test set.

From Table 2, it can be seen that CRU-RecNet has better retrieval performance on the test set compared to other models. Specifically, the MAE improves by 23.71% compared to U-Net. The MBE both underperforms on the test set, but CRU-RecNet still improves by 48.86% compared to U-Net. The RMSE ratio improves by 46.94%. And R improves by 3.81%. Compared to RESU-Net, MAE improves by 11.66%.MBE reduces underestimation by 47.29%.RMSE improves by 20.62%. Compared to DNN, MAE improves by 24.72%. And MBE reduces the underestimation by 60.12%. And RMSE improves by 42.83%. And R improves by 4.69%. These significant improvements highlight CRU-RecNet's ability to deliver higher accuracy and superior robustness under various conditions.

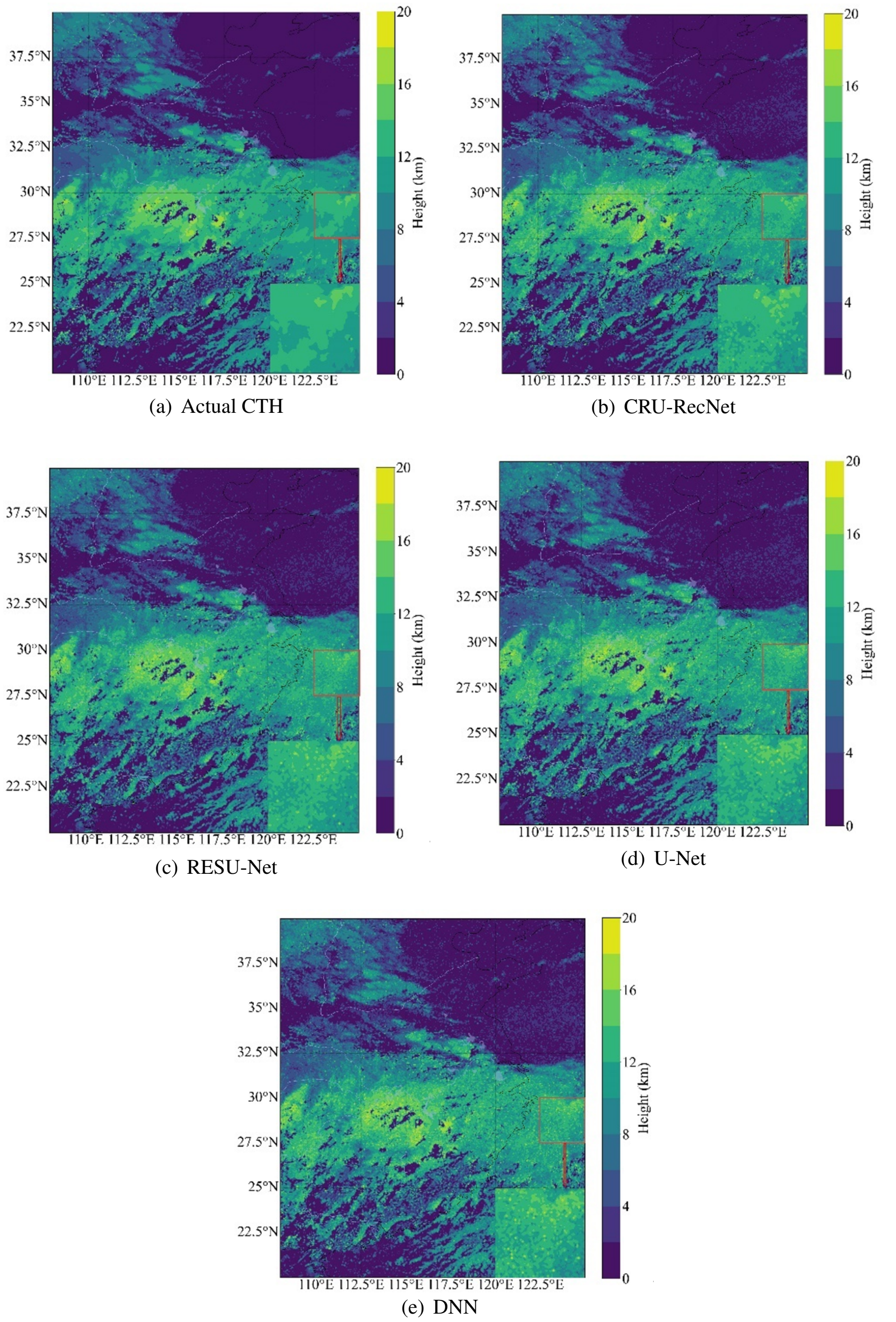


(a) Actual CTH

(b) CRU-RecNet

(c) RESU-Net

(d) U-Net

(e) DNN

Figure 4: Results of the July 7, 2020, 8:30 a.m. retrieval performance for each model

Figure 4 shows the retrieval results of various models for CTH on July 7, 2020, at 8:30 a.m. The results indicate that deep learning-based models effectively retrieve CTH using infrared channel data. Notably, the retrieval map produced by CRU-RecNet aligns most closely with the actual CTH map, demonstrating its superior ability to capture cloud-top features under complex atmospheric conditions.

Figure 5 illustrates the density scatter plots and probability density function plots of the retrieval results for each model on July 7, 2020. These plots clearly demonstrate the discrepancies between the retrieval data and the actual values of each model. As evidenced by the plots, the CRU-RecNet model exhibits the most optimal retrieval results. In particular, the CRU-RecNet model shows superior performance compared to the suboptimal model, with an MAE of 18.54%, an MBE of 4%, an RMSE of 21.78%, and a correlation R of 0.82% higher than the suboptimal model. Additionally, it is notable that the models demonstrate an overall tendency towards underestimation, both in the test set and in the retrieval cases. This phenomenon may be attributed to the absence of high cloud data, which could have otherwise provided a more accurate representation of the actual values.

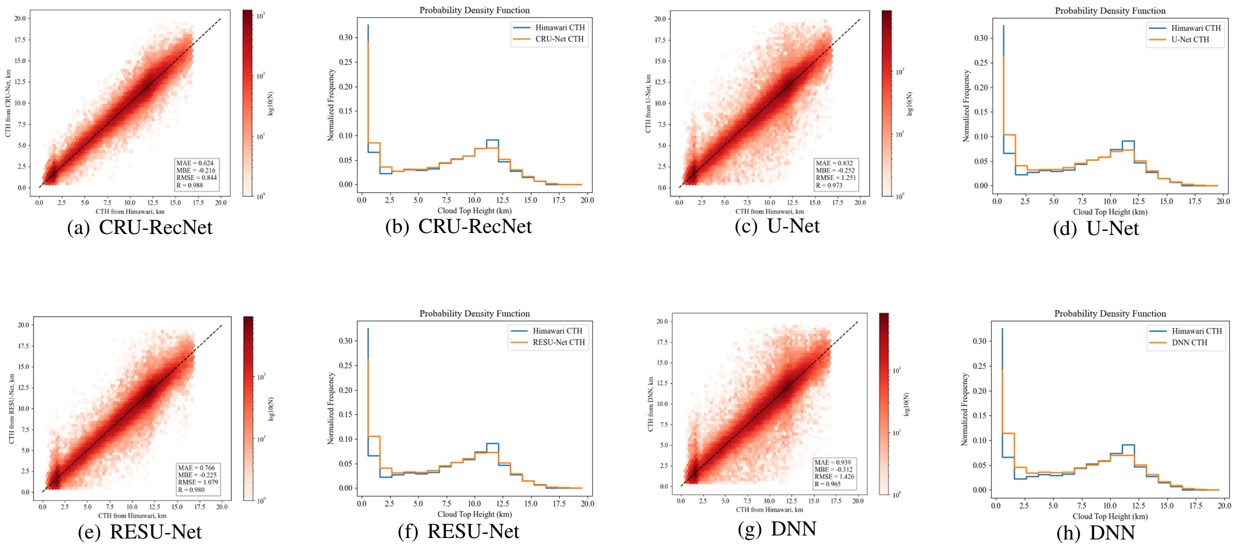


(a) CRU-RecNet (b) CRU-RecNet (c) U-Net (d) U-Net

(e) RESU-Net (f) RESU-Net (g) DNN (h) DNN

Figure 5: Density Scatter Plot and Probability Density Function of July 7, 2020 Retrieval Results for Each Model

This study employs nighttime CTH data from the CALIPSO satellite to evaluate the performance of each model under nighttime conditions. Figures 6(a) and 7(a) display the CALIPSO satellite trajectories during the data acquisition process, while Figures 6(b) and 7(b) present the nighttime CTH data alongside retrieval results for July 7, 2020, and January 6, 2022. The results indicate that although all models demonstrate acceptable performance in nighttime CTH retrieval, CRU-RecNet consistently achieves the best performance, with retrieval results that most closely match the actual data.

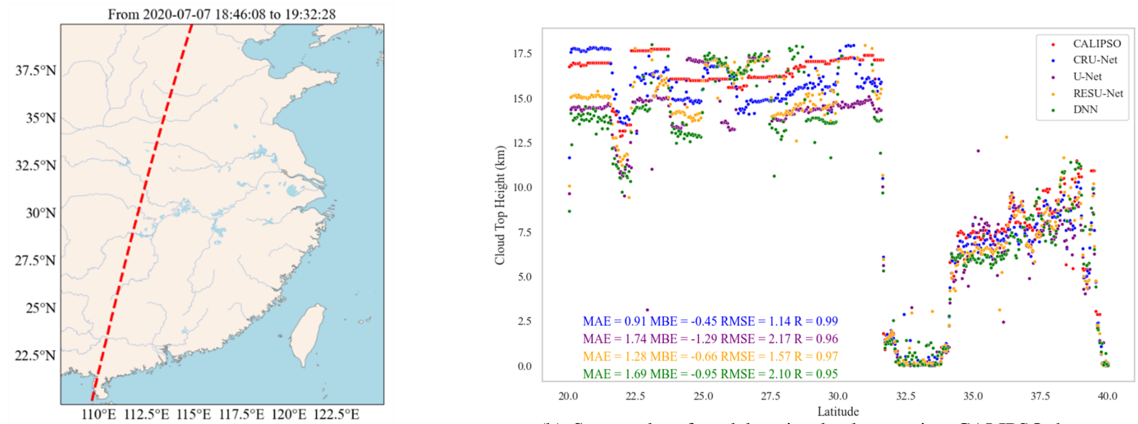


(a) Chart of the orbit of the CALIPSO satellite (b) Scatter plot of model retrieval values against CALIPSO data

Figure 6: July 7, 2020, model retrieval values with CALIPSO nighttime data profiles and CALIPSO trajectories

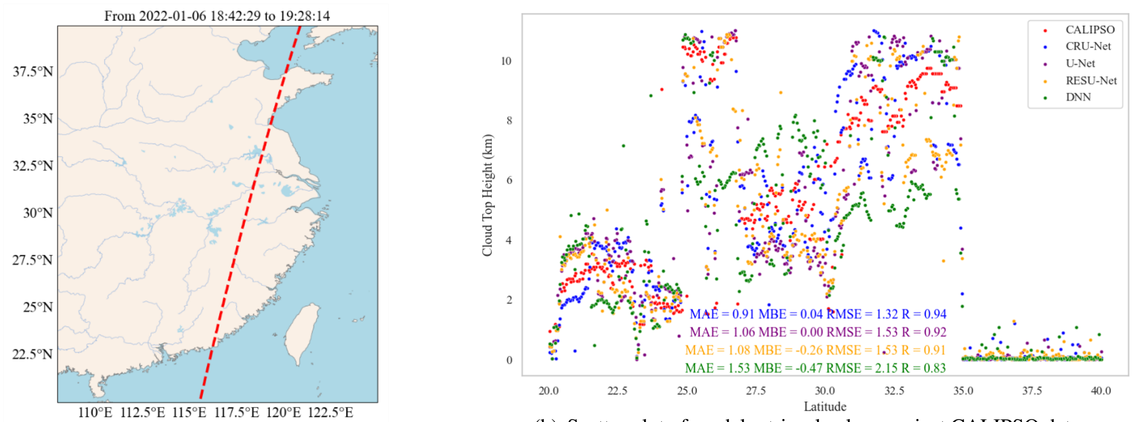


(a) Chart of the orbit of the CALIPSO satellite

(b) Scatter plot of model retrieval values against CALIPSO data

Figure 7: January 6, 2022, model retrieval values with CALIPSO nighttime data profiles and CALIPSO trajectories

The comparative experimental results and nighttime retrieval validations using CALIPSO data confirm that the CRU-RecNet model achieves highly efficient cloud-top height inversion during the daytime and maintains exceptional robustness under limited light conditions at night. Compared to other models, CRU-RecNet consistently demonstrates higher retrieval accuracy and reliability across various atmospheric scenarios.

### *4.6. Ablation experiments*

#### *4.6.1. Retrieval accuracy*

The objective of a series of ablation experiments on CRU-RecNet is to ascertain whether the designed modules can effectively enhance the model's retrieval performance. The U-Net model was used as the baseline for the removal of the MAM, the SAM, and the dual-decoding structure, which were evaluated exhaustively through quantitative analysis. In particular, CRU-RecNet (wo. MAM) represents the retrieval model in which the MAM has been removed, CRU-RecNet (wo. SAM) denotes the retrieval model in which the SAM has been removed, and CRU-RecNet (wo. DDM) denotes the removal of the dual decoding structure.

Table 3: Results of Ablation Experiments

| **Model name** | **MAE** | **MBE** | **RMSE** | **R** |
|---|---|---|---|---|
| U-Net | 0.894 | -0.265 | 1.416 | 0.946 |
| CRU-RecNet (wo. MAM) | 0.783 | -0.232 | 1.231 | 0.953 |
| CRU-RecNet (wo. SAM) | 0.749 | -0.187 | 1.012 | 0.968 |
| CRU-RecNet (wo. DDM) | 0.703 | -0.151 | 0.925 | 0.973 |
| **CRU-RecNet** | **0.682** | **-0.136** | **0.893** | **0.982** |

The quantitative evaluation results of the ablation experiment of CRU-RecNet are presented in Table 3. As a benchmark model, U-Net is capable of capturing the fundamental characteristics of CTH retrieval. However, it is deficient in its ability to discern intricate multi-scale features and long-distance correlations, necessitating enhancements to its performance. The removal of any component from the CRU-RecNet model resulted in a decline in performance across all evaluation metrics. In particular, the removal of MAM has the most significant impact on the model, indicating that MAM plays a pivotal role in capturing multi-scale features and reducing interference. This is evidenced by a 14.81%, 70.59%, 37.85%, and 2.95% decrease in the four ratings, respectively. The removal of SAM resulted in a reduction of 9.82%, 37.5%, 13.33%, and 1.43% in the four scores, respectively. This evidence substantiates the efficacy of the SAM in enhancing the model's capacity to capture long-range dependencies. The removal of the DDM resulted in a decrease of the four ratings by 3.08%, 11.03%, 3.58%, 3.58%, and 0.92%, respectively. This outcome substantiates the contribution of the DDM in restoring resolution and capturing detailed features, thereby enhancing the overall performance of the model.

*4.6.2. Recommendation performance*

To assess the impact of different modules in enhancing the recommendation performance of CRU-RecNet, we conducted a series of comparative experiments between the CRU-RecNet and U-Net models within the recommendation system. U-Net was used as the baseline model, and Precision@K and Recall@K were chosen as evaluation metrics. We also tested the effects of removing specific components from the CRU-RecNet architecture to conduct a detailed quantitative evaluation. Specifically, CRU-RecNet (wo. MAM) represents the model with the MAM removed, and CRU-RecNet (wo. SAM) represents the model without the SAM.

Table 4 shows the quantitative evaluation results for each model in the recommendation task:

Table 4: Performance Comparison of CRU-RecNet and U-Net in Recommendation System

| **Model Name** | **Precision@K** | **Recall@K** |
|---|---|---|
| U-Net | 0.734 | 0.682 |
| CRU-RecNet (wo. MAM) | 0.765 | 0.723 |
| CRU-RecNet (wo. SAM) | 0.792 | 0.751 |
| **CRU-RecNet (Complete)** | **0.814** | **0.782** |

From the data, it is evident that as the baseline model, U-Net provides a certain level of recommendation performance but is limited in its ability to capture detailed user preference features. When any of the components in CRU-RecNet are removed, the evaluation metrics drop. Specifically, removing the MAM led to a 6.02% and 5.86% decrease in Precision@K and Recall@K, respectively, indicating that capturing multi-scale features plays a crucial role in improving recommendation precision and coverage. When the SAM was removed, Precision@K and Recall@K dropped by 2.7% and 3.9%, respectively, highlighting the importance of SAM in capturing global user behavior patterns. With all modules intact, the complete CRU-RecNet model outperforms U-Net in both Precision@K and Recall@K, demonstrating that the introduction of multi-scale attention and self-attention mechanisms significantly enhances the accuracy and comprehensiveness of the recommendation system.

## 5. Conclusion

In this paper, we proposed CRU-RecNet, a novel model that integrates multi-scale attention and self-attention mechanisms for accurate CTH retrieval and IMSR. By leveraging CTH data, the model enhances weather forecasting accuracy and delivers personalized weather services. Experimental results demonstrated that CRU-RecNet significantly improves both CTH retrieval and recommendation performance compared to existing methods. The integration of attention mechanisms enables the model to capture multi-scale atmospheric patterns and long-range dependencies, making it well-suited for dynamic, real-time meteorological applications.

## Acknowledgments

This work was supported in part by the National Natural Science Foundation of China under Grant 92267104 and Grant 62372242 and Jiangsu Provincial Major Project on Basic Research of Cutting-edge and Leading Technologies under Grant No. BK20232032.

## References

[1] W. Liu, C. Chen, X. Liao, M. Hu, Y. Tan, F. Wang, X. Zheng, Y. S. Ong, Learning accurate and bidirectional transformation via dynamic embedding transportation for cross-domain recommendation, Proceedings of the AAAI Conference on Artificial Intelligence 38 (8) (2024) 8815–8823. doi:10.1609/aaai.v38i8.28728.

[2] J. Zhang, W. Zhu, B. J. Ahn, Y. Zhou, Composite recommendation of artworks in e-commerce based on user keyword-driven correlation graph search, Tsinghua Science and Technology 29 (1) (2024) 174–184. doi:10.26599/TST.2023.9010012.
[3] A. Mutemi, F. Bacao, E-commerce fraud detection based on machine learning techniques: Systematic literature review, Big Data Mining and Analytics 7 (2) (2024) 419–444. doi:10.26599/BDMA.2023.9020023.
[4] C. Hu, W. Fan, E. Zeng, Z. Hang, F. Wang, L. Qi, M. Z. A. Bhuiyan, Digital twin-assisted real-time traffic data prediction method for 5g-enabled internet of vehicles, IEEE Transactions on Industrial Informatics 18 (4) (2022) 2811–2819. doi:10.1109/TII.2021.3083596.
[5] M. Min, J. Li, F. Wang, Z. Liu, W. P. Menzel, Retrieval of cloud top properties from advanced geostationary satellite imager measurements based on machine learning algorithms, Remote Sensing of Environment 239 (2020) 111616. doi:10.1016/j.rse.2019.111616.
[6] Y. Liu, Y. Zhang, X. Mao, X. Zhou, J. Chang, W. Wang, P. Wang, L. Qi, Lithological facies classification using attention-based gated recurrent unit, Tsinghua Science and Technology 29 (4) (2024) 1206–1218. doi:10.26599/TST.2023.9010077.
[7] F. Fei, S. Li, H. Dai, C. Hu, W. Dou, Q. Ni, A k-anonymity based schema for location privacy preservation, IEEE Transactions on Sustainable Computing 4 (2) (2019) 156–167. doi:10.1109/TSUSC.2017.2733018.
[8] W. Dou, W. Tang, X. Wu, L. Qi, X. Xu, X. Zhang, C. Hu, An insurance theory based optimal cyber-insurance contract against moral hazard, Information Sciences 527 (2020) 576–589. doi:10.1016/j.ins.2018.12.051.
[9] L. Chen, Y. Li, H. Liu, H. Guo, Node and edge joint embedding for heterogeneous information network, Big Data Mining and Analytics 7 (3) (2024) 730–752. doi:10.26599/BDMA.2023.9020037.
[10] R. A. Frey, S. A. Ackerman, Y. Liu, K. I. Strabala, H. Zhang, J. R. Key, X. Wang, Cloud detection with modis. part i: Improvements in the modis cloud mask for collection 5, Journal of Atmospheric and Oceanic Technology 25 (7) (2008) 1057 – 1072. doi:10.1175/2008JTECHA1052.1.
[11] T. Deutschmann, S. Beirle, U. Frieß, M. Grzegorski, C. Kern, L. Kritten, U. Platt, C. Prados-Román, J. Pukı¯te, T. Wagner, B. Werner, K. Pfeilsticker, The monte carlo atmospheric radiative transfer model mcartim: Introduction and validation of jacobians and 3d features, Journal of Quantitative Spectroscopy and Radiative Transfer 112 (6) (2011) 1119–1137. doi:10.1016/j.jqsrt.2010.12.009.
[12] R. Gu, S. Wang, H. Dai, X. Chen, Z. Wang, W. Bao, J. Zheng, Y. Tu, Y. Huang, L. Qi, X. Xu, W. Dou, G. Chen, Fluid-shuttle: Efficient cloud data transmission based on serverless computing compression, IEEE/ACM Transactions on Networking 32 (6) (2024) 4554–4569. doi:10.1109/TNET.2024.3402561.
[13] Q. Sun, L. Shi, L. Liu, Z. Han, L. Jiang, Y. Wu, Y. Zhao, A novel recommendation algorithm integrates resource allocation and resource transfer in weighted bipartite network, Big Data Mining and Analytics 7 (2) (2024) 357–370. doi:10.26599/BDMA.2023.9020029.
[14] K. Taha, P. D. Yoo, C. Yeun, A. Taha, Empirical and experimental perspectives on big data in recommendation systems: A comprehensive survey, Big Data Mining and Analytics 7 (3) (2024) 964–1014. doi:10.26599/BDMA.2024.9020009.
[15] W. Lin, M. Zhu, X. Zhou, R. Zhang, X. Zhao, S. Shen, L. Sun, A deep neural collaborative filtering based service recommendation method with multi-source data for smart cloud-edge collaboration applications, Tsinghua Science and Technology 29 (3) (2024) 897–910. doi:10.26599/TST.2023.9010050.
[16] F. Wang, C. Chen, W. Liu, T. Fan, X. Liao, Y. Tan, L. Qi, X. Zheng, Ce-rcfr: Robust counterfactual regression for consensus-enabled treatment effect estimation, in: Proceedings of the 30th ACM SIGKDD Conference on Knowledge Discovery and Data Mining, KDD '24, Association for Computing Machinery, 2024, p. 3013–3023. doi:10.1145/3637528.3672054.
[17] J. Liu, H. Gao, C. Yang, C. Shi, T. Yang, H. Cheng, Q. Xie, X. Wang, D. Wang, Heterogeneous spatio-temporal graph contrastive learning for point-of-interest recommendation, Tsinghua Science and Technology 30 (1) (2025) 186–197. doi:10.26599/TST.2023.9010148.
[18] N. Siddique, S. Paheding, C. P. Elkin, V. Devabhaktuni, U-net and its variants for medical image segmentation: A review of theory and applications, IEEE Access 9 (2021) 82031–82057. doi:10.1109/ACCESS.2021.3086020.
[19] J. H. Jeppesen, R. H. Jacobsen, F. Inceoglu, T. S. Toftegaard, A cloud detection algorithm for satellite imagery based on deep learning, Remote Sensing of Environment 229 (2019) 247–259. doi:10.1016/j.rse.2019.03.039.
[20] X. Tan, K. Ma, F. Dou, A convolutional neural network and attention-based retrieval of temperature profile for a satellite hyperspectral microwave sensor, Atmosphere 15 (2). doi:10.3390/atmos15020235.
[21] H. Mansourifar, A. Moskovitz, B. Klingensmith, D. Mintas, S. J. Simske, Gan-based satellite imaging: A survey on techniques and applications, IEEE Access 10 (2022) 118123–118140. doi:10.1109/ACCESS.2022.3221123.
[22] M. R. Ehsani, A. Zarei, H. V. Gupta, K. Barnard, E. Lyons, A. Behrangi, Nowcasting-nets: Representation learning to mitigate latency gap of satellite precipitation products using convolutional and recurrent neural networks, IEEE Transactions on Geoscience and Remote Sensing 60 (2022) 1–21. doi:10.1109/TGRS.2022.3158888.
[23] L. Qi, R. Wang, C. Hu, S. Li, Q. He, X. Xu, Time-aware distributed service recommendation with privacy-preservation, Information Sciences 480 (2019) 354–364. doi:10.1016/j.ins.2018.11.030.
[24] Y. Zhao, J. Chen, Vector-indistinguishability: Location dependency based privacy protection for successive location data, IEEE Transactions on Computers 73 (4) (2024) 970–979. doi:10.1109/TC.2023.3236900.
[25] F. Sun, J. Liu, J. Wu, C. Pei, X. Lin, W. Ou, P. Jiang, Bert4rec: Sequential recommendation with bidirectional encoder representations from transformer, in: Proceedings of the 28th ACM international conference on information and knowledge management, 2019, pp. 1441–1450. doi:10.1145/3357384.3357895.
[26] Y.-C. Chen, Y.-L. Chen, C.-H. Hsu, G-transrec: A transformer-based next-item recommendation with time prediction, IEEE Transactions on Computational Social Systems 11 (3) (2024) 4175–4188. doi:10.1109/TCSS.2024.3354315.
[27] G. Zhou, X. Zhu, C. Song, Y. Fan, H. Zhu, X. Ma, Y. Yan, J. Jin, H. Li, K. Gai, Deep interest network for click-through rate prediction, in: Proceedings of the 24th ACM SIGKDD international conference on knowledge discovery & data mining, 2018, pp. 1059–1068. doi:10.1145/3219819.3219823.
[28] X. Xu, H. Dong, H. Xiang, X. Hu, X. Li, X. Xia, X. Zhang, L. Qi, W. Dou, C2lrec: Causal contrastive learning for user cold-start recommendation with social variable, ACM Trans. Inf. Syst.doi:10.1145/3711858.
[29] W. Huang, J. Wu, W. Song, Z. Wang, Cross attention fusion for knowledge graph optimized recommendation, Applied Intelligence (2022) 1–10doi:10.1007/s10489-021-02930-1.
[30] X. Xu, F. Wu, M. Bilal, X. Xia, W. Dou, L. Yao, W. Zhong, Xrl-shap-cache: an explainable reinforcement learning approach for intelligent

edge service caching in content delivery networks, Science China Information Sciences 67 (7) (2024) 170303. doi:10.1007/s11432-023-3987-y.

[31] H. Xiang, X. Zhang, X. Xu, A. Beheshti, L. Qi, Y. Hong, W. Dou, Federated learning-based anomaly detection with isolation forest in the iot-edge continuum, ACM Trans. Multimedia Comput. Commun. Appl.Just Accepted. doi:10.1145/3702995.

[32] X. Xu, X. Zhou, X. Zhou, M. Bilal, L. Qi, X. Xia, W. Dou, Distributed edge caching for zero trust-enabled connected and automated vehicles: A multi-agent reinforcement learning approach, IEEE Wireless Communications 31 (2) (2024) 36–41. doi:10.1109/MWC.001.2300414.

[33] X. Zhao, L. Xia, L. Zhang, Z. Ding, D. Yin, J. Tang, Deep reinforcement learning for page-wise recommendations, in: Proceedings of the 12th ACM conference on recommender systems, 2018, pp. 95–103. doi:10.1145/3240323.3240374.

[34] A. B. H. Ali, S. B. Ahmed, Rlrec: Towards reinforcement learning-based dynamic design of reconfiguration control, Procedia Computer Science 225 (2023) 3670–3680. doi:10.1016/j.procs.2023.10.362.

[35] J. Liu, Y. Zhang, X. Wang, Y. Deng, X. Wu, Dynamic pricing on e-commerce platform with deep reinforcement learning: A field experiment, arXiv preprint arXiv:1912.02572.

[36] M. Mohammadi, A. Al-Fuqaha, M. Guizani, J.-S. Oh, Semisupervised deep reinforcement learning in support of iot and smart city services, IEEE Internet of Things Journal 5 (2) (2018) 624–635. doi:10.1109/JIOT.2017.2712560.

[37] A. Amelio, G. Bonifazi, F. Cauteruccio, E. Corradini, M. Marchetti, D. Ursino, L. Virgili, Representation and compression of residual neural networks through a multilayer network based approach, Expert Systems with Applications 215 (2023) 119391. doi:10.1016/j.eswa.2022.119391.

[38] C. A. Aguni, L. M. Sato, E. T. Midorikawa, Mcmpi: A library with elasticity for multi-domain and public cloud environments, Concurrency and Computation: Practice and Experience 36 (18) (2024) e8149. doi:10.1002/cpe.8149.

[39] B.-h. M. Portella, H. d. M. J. Barbosa, Climatology and trends of cirrus geometrical and optical properties in the amazon region from 7-yr of calipso observations, Atmospheric Research 299 (2024) 107167. doi:10.1016/j.atmosres.2023.107167.

[40] R. Onishi, T. Hoshino, H. Kawashima, Epo-r: An efficient garbage collection scheme for long-term transactions, Concurrency and Computation: Practice and Experience 36 (17) (2024) e8134. doi:10.1002/cpe.8134.

[41] K. He, X. Zhang, S. Ren, J. Sun, Delving deep into rectifiers: Surpassing human-level performance on imagenet classification, in: Proceedings of the IEEE international conference on computer vision, 2015, pp. 1026–1034. doi:10.1109/ICCV.2015.123.

[42] X. Wang, H. Iwabuchi, T. Yamashita, Cloud identification and property retrieval from himawari-8 infrared measurements via a deep neural network, Remote Sensing of Environment 275 (2022) 113026. doi:10.1016/j.rse.2022.113026.

[43] Q. Wang, C. Zhou, X. Zhuge, C. Liu, F. Weng, M. Wang, Retrieval of cloud properties from thermal infrared radiometry using convolutional neural network, Remote Sensing of Environment 278 (2022) 113079. doi:10.1016/j.rse.2022.113079.

[44] Z. Zhao, F. Zhang, Q. Wu, Z. Li, X. Tong, J. Li, W. Han, Cloud identification and properties retrieval of the fengyun-4a satellite using a resunet model, IEEE Transactions on Geoscience and Remote Sensing 61 (2023) 1–18. doi:10.1109/TGRS.2023.3252023.